applied sciences

MDPI

Article

Practical Approach for Assessing Wetting-Induced Slope Failure

Glenn Adriel Adiguna [1], Martin Wijaya [1], Paulus Pramono Rahardjo [1], Andy Sugianto [2], Alfrendo Satyanaga [3,*] and Abdul Halim Hamdany [4]

1 Faculty of Engineering, Civil Engineering Department, Universitas Katolik Parahyangan, Jl. Ciumbuleuit No. 94, Bandung City 40141, Indonesia
2 Engineering Division, P.T. Geotechnical Engineering Consultant, Jl. Lembah Sukaresmi 1 No 11, Bandung City 40162, Indonesia
3 Department of Civil and Environmental Engineering, Nazarbayev University, 53, Kabanbay Batyr Ave, Nur-Sultan 010000, Kazakhstan
4 Department of Civil Engineering, University of Indonesia, Depok City 16424, Indonesia
* Correspondence: alfrendo.satyanaga@nu.edu.kz

Abstract: Ignoring the role of soil suction and implementing unsaturated soil mechanics when assessing slope stability in Indonesia is a common practice. One of the main reasons is due to the precognition that incorporating soil suction means using higher shear strength, which leads to less conservative analysis, while it is difficult to practically obtain accurate input parameters for unsaturated soil analysis. However, a number of slope failures occur all over the world due to rainfall, which becomes evidence that ignoring the role of soil suction may not necessarily lead to a conservative result. On 9 January 2021, rainfall-induced slope failure occurred at Cimanggung after four hours of heavy rainfall and killed 32 people. Many of them were injured, and houses were destroyed. This event shows the significance of considering the interaction between infiltration and soil suction when conducting slope stability analysis. Difficulties in obtaining input parameters for unsaturated soil analysis experimentally hindered practitioners in applying unsaturated soil mechanics. While the parameters can be estimated, it is always of question whether the estimated parameters are sufficiently accurate for practical purposes. In this paper, conventional site investigations were carried out while unsaturated soil parameters were estimated to study the mechanism which triggers the landslide that occurred at Cimanggung. It will be shown that estimating unsaturated soil parameters can be practically accurate and manage to capture the failure mechanism such as critical rainfall duration and critical slip surface.

Keywords: rainfall-induced slope failure; Cimanggung; Indonesia; slope stability; unsaturated soil

Citation: Adiguna, G.A.; Wijaya, M.; Rahardjo, P.P.; Sugianto, A.; Satyanaga, A.; Hamdany, A.H. Practical Approach for Assessing Wetting-Induced Slope Failure. *Appl. Sci.* **2023**, *13*, 1811. https://doi.org/10.3390/app13031811

Academic Editor: Daniel Dias

Received: 13 January 2023
Revised: 22 January 2023
Accepted: 28 January 2023
Published: 31 January 2023

1. Introduction

The existence and role of negative pore-water pressure above the ground-water table is commonly ignored. The reason for such ignorance is due to the assumption that there is no need for such science [1]. Hence, analysing slope stability is conventionally carried out by assuming zero pore water pressure above the ground-water table and positive pore-water pressure below the ground-water table. The position of the ground-water table is assumed based on instrumentation or borehole data and the effect of climates is taken care of by assuming a higher ground-water level. The role of suction is commonly viewed to increase soil shear strength [2] which then leads to less conservative analysis. However, a number of landslides occurred due rainfall infiltration [3,4] which then raised a question whether the conventional approach which ignores the role of soil suction has been sufficiently conservative. Rahardjo, Ong [5] have shown that water-table location is secondary in rainfall-induced slope failure, especially when the water table is sufficiently deep. Hence, slightly raising the water table might not be sufficient as the effect of infiltration is located at a shallower depth.

Rainfall infiltration causes an increase in pore-water pressure or a reduction in soil suction, which then leads to an increase in degree of saturation and the formation of a perched water table or increase in ground-water level [6], which leads to a reduction in soil shear strength which triggers slope failure [1,7–10]. Such a phenomenon has been observed all over the world, such as an increase in ground-water level which triggered a deep-seated landslide in Zhejian, China [11,12], and formation of a perched water table which induced a landslide in Shilong, India [13]. The role of suction in altering soil permeability [14,15] is very important in controlling the formation of perched water table and changes in ground-water level.

However, rainfall is not the only triggering mechanism which causes slope failure. Soil properties and slope geometry also take an important role in determining whether the slope failure is susceptible to landslide [9,16]. Brand [17] shows that the effect of rainfall in Hong Kong is not significant due to high soil permeability. Hence, slopes geometry with different soil properties or geological formation and under different ground-water table positions will have different critical rainfall infiltration rates and durations [18]. The problems become especially severe when the slope is located on top of expansive soils as described in Yao, Li [19].

Unsaturated soil mechanics allow a more realistic determination of the perch water table or an increase in ground-water level which is transient by considering the interaction between climates, soil properties, and slope geometry, which can be more conservative than conventional approach. It also allowed us to determine critical rainfall infiltration and durations which can be important in assessing whether the slope of interest is prone to failure due to rainfall or not.

In order to conduct unsaturated slope stability analysis, it is necessary to have a soil–water characteristic curve (SWCC), permeability function of unsaturated soils, and shear strength of unsaturated soils. SWCC describes the amount of water that can be retained by the soil pores at a certain matric suction value and has a very important role in determining or estimating shear strength, compressibility, and permeability of unsaturated soils [20,21]. However, directly measuring SWCC is difficult [22] as it is not part of routine geotechnical practice especially in Indonesia. Moreover, when the SWCC test is conducted, it is important to note that experimental and field SWCC are usually different [22,23]. Hence, it is very difficult to directly conduct SWCC tests and obtain SWCC for each soil layer. However, a rough estimate of SWCC is generally sufficient for unsaturated soil analysis [1] due to the significant order of difference between the SWCC of different soil types. Hence, a number of methods to estimate SWCC have been proposed, such as: (1) estimating SWCC based on basic soil properties [24–26]; (2) SWCC database, i.e SoilVision [27] and unsaturated soil hydraulic database (UNSODA) [28,29]; or (3) SWCC sample data available in commercial software (i.e., Geostudio or MIDAS GTS NX).

Estimating SWCC based on basic soil properties is perhaps the easiest to employ as it does not require any database and some of them have been incorporated in the commercial software. For instance, the Aubertin, Mbonimpa [25] method or modified Kovacs [24] can be used to determine SWCC based on basic geotechnical properties and have been employed in Geostudio. Aubertin, Mbonimpa [25] assume that there is a distinction between the adhesion of water with a solid surface and surface tension at the interface with air causing capillary retention. These adhesion forces and capillary forces are acting simultaneously to create suction in the soil. The equation initially determined the degree of saturation-based SWCC (SWCC-S) and then converted to volumetric water-content-based SWCC (SWCC-θ). The equation for the degree of saturation is provided in Equation (1):

$$S_r = \frac{\theta}{n} = S_c + S_a^*(1 - S_c) \tag{1}$$

where S_c is the degree of saturation due to capillary forces, and S_a^* is the truncated values of the degree of saturation due to adhesive forces. The method to make sure that the adhesion component does not exceed unity at low suction S_a^* is defined in Equation (2):

$$S_a^* = 1 - \langle 1 - S_a \rangle \tag{2}$$

The contribution of capillary component (which mainly contributed at low suction) to the total degree of saturation is defined in Equation (3):

$$S_c = 1 - \left[(h_{co}/\Psi)^2 + 1 \right]^m exp\left[-m (h_{co}/\Psi)^2 \right] \tag{3}$$

where m is the pore-size distribution parameter, Ψ is the matric suction, and h_{co} is the equivalent capillary rise for granular soils which is provided in Equation (4):

$$h_{co} = \frac{b}{eD_{10}} \tag{4}$$

with:

$$b = \frac{0.75}{1.17 \log C_u + 1} \tag{5}$$

where C_u is the coefficient of uniformity. For plastic cohesive, h_{co} is defined as:

$$h_{co} = \frac{\xi}{e} w_L^{1.45} \tag{6}$$

where w_L is the liquid limit and ξ is a constant approximately equal to 402.2 cm^2. The contribution of the adhesion component (which mainly contributed at higher suction) to the total degree of saturation is defined as:

$$S_a = a_c C\Psi \frac{(h_{co}/\Psi_n)^{2/3}}{e^{1/3} (\Psi/\Psi_n)^{1/6}} \tag{7}$$

where a_c is the fitting parameter, Ψ_n is the suction term to ensure dimensionless component, and C_Ψ is the correction function from Fredlund and Xing [30] which is defined as:

$$C_\Psi = 1 - \frac{\ln(1 + \Psi/\Psi_r)}{\ln(1 + \Psi_0/\Psi_r)} \tag{8}$$

where Ψ_r is the suction corresponding to residual water content.

Determination of the unsaturated permeability function is more difficult and tedious than obtaining SWCC. Hence, it is quite common to the estimate permeability function for unsaturated soil by using the Fredlund, Xing [31] statistical method, which is defined as follows:

$$k_r(\psi) = \frac{\int_{\ln \psi}^{\ln s_u} \frac{w(e^y) - w(s)}{e^y} w'(e^y) dy}{\int_{\ln s_L}^{\ln s_u} \frac{w(e^y) - w(s_L)}{e^y} w'(e^y) dy} \tag{9}$$

where k_r is the relative coefficient of permeability, and w is the water content that can be either gravimetric water content, volumetric water content, or degree of saturation. ψ is soil suction, s_L is the suction at the lower limit of integration (corresponding to gravimetric water content $w(s_L)$) and is commonly taken as the air-entry value (AEV), s_U is the soil suction at the upper limit of integration (corresponding to gravimetric water content

w_U) and is commonly taken as residual soil suction [1] or 1 GPa [14]. The coefficient of permeability for unsaturated soil (k) can then be defined as:

$$k = k_s k_r(s) \tag{10}$$

The shear strength (τ) of unsaturated soil is commonly represented by using extended Mohr–Coulomb [2], which can be written as:

$$\tau = c' + (\sigma - u_a)\tan\phi' + (u_a - u_w)\tan\phi^b \tag{11}$$

where c' is effective cohesion, $(\sigma - u_a)$ is net normal stress, ϕ' is the effective friction angle, u_a is pore-air pressure, u_w is pore-water pressure, and ϕ^b is the angle representing change in shear strength due to change in soil suction. Based on some experimental values, ϕ^b ranged from 1/3 to 2/3 of the ϕ.

Estimating unsaturated soil properties is a way to make unsaturated soil mechanics become practically applicable for routine industrial practice. However, it is important to verify whether the estimated parameter is able to capture the mechanism of slope failure. Back analysis of slope failure is one of the tools used to verify whether such a routine can be adopted. Based on the issue which has been raised in this paper, the objective of this paper is to verify whether estimating unsaturated soil properties based on an empirical approach is sufficient to capture the failure mechanism of rainfall-induced slope failure. Cimanggung slope failure will be used as a case study in this paper.

2. Site Overview of Cimanggung Slope Failure

On 9 January 2021, catastrophic slope failures occurred at Cihanjuang village, located at Cimanggung, Sumedang, West Java. It is interesting to note that, for more than 20 years, slope failure never occurred in this area. SBG Housing (*Perumahan SBG*) is located at the crown of the slope while Daud housing (*Perumahan Daud*) is located at the body of the slope, as shown in Figure 1.

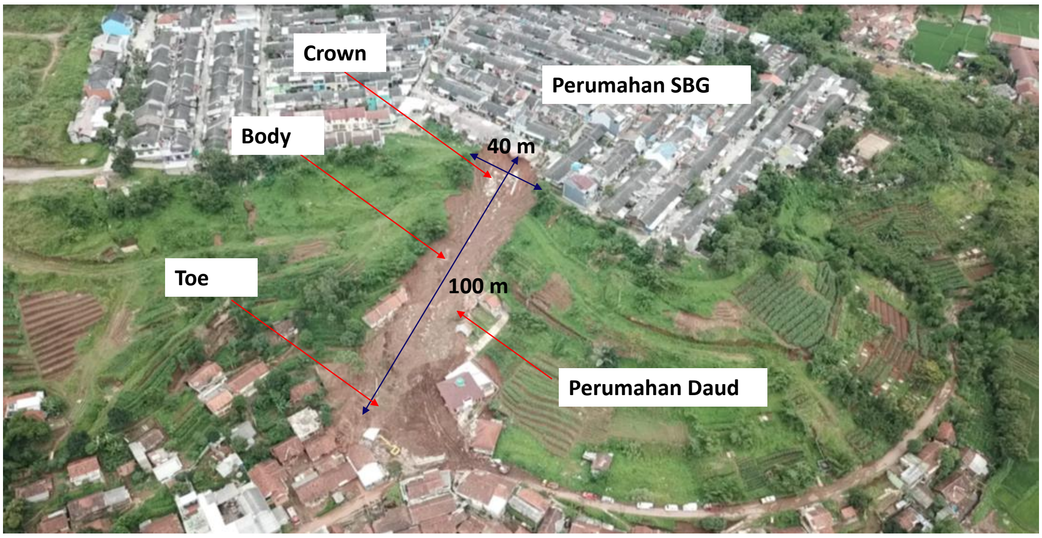

Figure 1. Post-failure slope conditions.

According to UInspire [32], 32 people died, 3 people were heavily injured, 22 people were lightly injured, while 8 people were missing. A total of 24 houses were completely destroyed, 5 houses were heavily damaged, 1 school, and 1 mosque were destroyed. Figure 2 shows the example of the destruction caused by the slope failure. The housing complex has been there for more than 25 years without any effect from slope failure which makes the citizens wonder at the causes of slope failure.

(**a**)

(**b**)

Figure 2. Destruction caused by the slope failure ((**a**) shows destruction of house located at the edge of the slope; (**b**) shows buried house at the bottom of the slope).

According to the witnesses, slope failure occurred after more than four hours of heavy rainfall which might be the major cause of the slope failure. According to several ground stations around the slope area [32], rainfall during the slope failure was as follows:

(a) Jatinangor district (143 mm/day);
(b) UNPAD Jatinangor (99 mm/day);
(c) Tanjung Sari (104 mm/day);
(d) AWS Cikancung (69.8 mm/day).

The data shows some variability and, as hourly rainfall data is not available at the site, it is difficult to accurately determine the actual infiltration rate and duration.

Another aspect which is worth considering is the possibility that drainage household capacity was exceeded. According to the site observation, household drainage, which is commonly located in front of the citizen housing, which is shown in Figure 3, is designed for 5 years of rainfall which appears to be insufficient. Hence, water floods and flow from the housing complex to the slope triggered the first landslide and damaged the drainage pipe located at the crown of the slope, as indicated in Figure 4. It is important to note that the first landslide was located below the drainage pipe. Hence, it will be evaluated whether the slope failure was only due to the rainfall or also due to the failure of the drainage system which caused overtopping or flooding at the crown of the slope.

In order to conduct proper back analysis, accurate geometry of the sliding plane or the post-failure slope geometry is very important. However, obtaining post-failure geometry might be hazardous as the site might remain unstable for the operator. Due to the development of the photogrammetry technique, it is now possible to generate a 3D slope model from a series of overlapping photographs by using aerial reconnaissance using an unmanned aerial vehicle or UAV [33–35]. By using UAV, post-geometry slope failure can now be determined accurately from a safe distance within a day.

Figure 3. Household drainage.

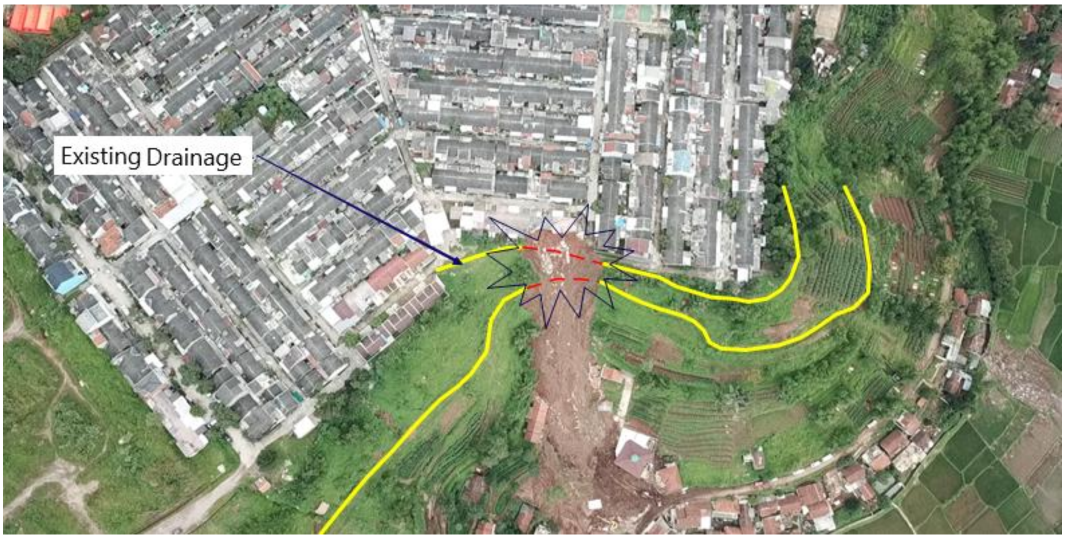

Figure 4. Waterflow and overtopping at the crown of the slope.

3. Materials and Methods

In order to study the rainfall-induced slope failure at Cimanggung, conventional site investigations were carried out, while unsaturated soil parameters were estimated. For the conventional site investigations, nine cone penetration tests (CPT) and three boreholes (BH) along with the standard penetration test (SPT) and undisturbed soil samplings were conducted. Piezometer was also installed at a 15 m depth. According to the site inspection, soils located around the slope consisted of clayey silt and gravels. Soils at the site were residual soils from Gunungapi Muda Rock which consist of tuff, lapilli, breccia, lava, and agglomerate. Ground-water levels were located approximately 20.5 m near the slope locations.

Location of the boreholes, piezometer, and CPT are shown in Figure 5 and are summarized in Table 1, while laboratory test data are summarized in Table 2. Figure 6 shows the soil stratification based on the borehole data. In the simulation, three soil layers were modelled. The upper layer was clayey silt where the sliding plane was located. All samples for laboratory tests were located in this layer, and it is shown that the soil properties were quite variable. However, it is important to note that the sliding plane was located at the first layer and hence, more emphasize was given to the first layer. Three triaxial consolidated undrained (TX-CU) tests were conducted on the three samples obtained from this layer. The range of effective cohesion was from 10 to 12 kPa, while the friction angle (ϕ') ranged from 35° to 37°. The value of ϕ appeared to be relatively high. One of the possible reasons was the soil, which is above the sliding plane, might have been colluvium and, hence, may have had lower ϕ. In the simulation, ϕ was back analysis such that the slip surface from the simulation and the actual slip surface matched, while ϕ^b was always taken as $1/2\phi$. The middle layer was very stiff clayey silt where only standard penetration test (SPT) N values were available. The SPT N value ranged from 25 to 32. S_u = 6 N is commonly adopted in Indonesia. By averaging the SPT N value, the total stress analysis with undrained shear strength equaled 170 kPa, which was adopted for the middle layer. Total stress analysis for the second layer was sufficient as the sliding plane was located at the first layer. Table 3 summarizes the parameters adopted in the simulation.

Figure 5. Borehole (BH-1 to BH-3), piezometer (Pz-1), and CPT (S1 to S9) locations.

Table 1. Boreholes and CPT coordinates.

BH	Coordinate: UTM 48 M		Elevation (m)	Depth (m)	GWL
	Easting	Northing			(m)
BH-1	811,380	9,230,325	732.29	18	*
BH-2	811,427	9,230,270	728.95	24	20.5
BH-3	811,421	9,230,173	726.62	9.5	8.5
S-01	811,427	9,230,263	729.08	7.6	-
S-02	811,446	9,230,237	731.51	9.4	-
S-03	811,432	9,230,218	726.88	5.0	-
S-04	811,411	9,230,259	719.27	3.2	-
S-05	811,353	9,230,304	716.06	5.0	-
S-06	811,414	9,230,142	722.58	4.0	-
S-07	811,413	9,230,244	712.67	5.2	-
S-08	811,413	9,230,228	715.21	3.8	-
S-09	811,355	9,230,200	696.07	3.4	-

* The ground water table is not detected.

Table 2. Properties of soils.

Borehole No.		BH-01	BH-02	BH-03
Sample Depth, m		6.00–6.50	2.50–3.00	2.00–2.50
Specific Gravity, Gs		2.58	2.55	2.53
Liquid Limit (w_L)		46.56	-	53.71
Plastic Limit (w_P)		31.20	-	31.18
Index Plasticity (IP)		15.36	-	22.53
Wet Density, gr/cm^3		1.77	1.88	1.77
Dry Density, gr/cm^3		1.25	1.45	1.26
Natural Water Content, %		40.41	30.12	36.47
Void Ratio, e		1.06	0.76	1.00
Porosity, n		0.52	0.43	0.50
Grain Size	Gravel, %	0.00	15.72	0.00
	Coarse Sand, %	4.13	11.77	0.66
	Medium Sand, %	8.41	13.59	4.04
	Fine Sand, %	15.96	19.46	11.13
	Silt, %	38.80	26.13	43.62
	Clay, %	32.70	13.33	40.55

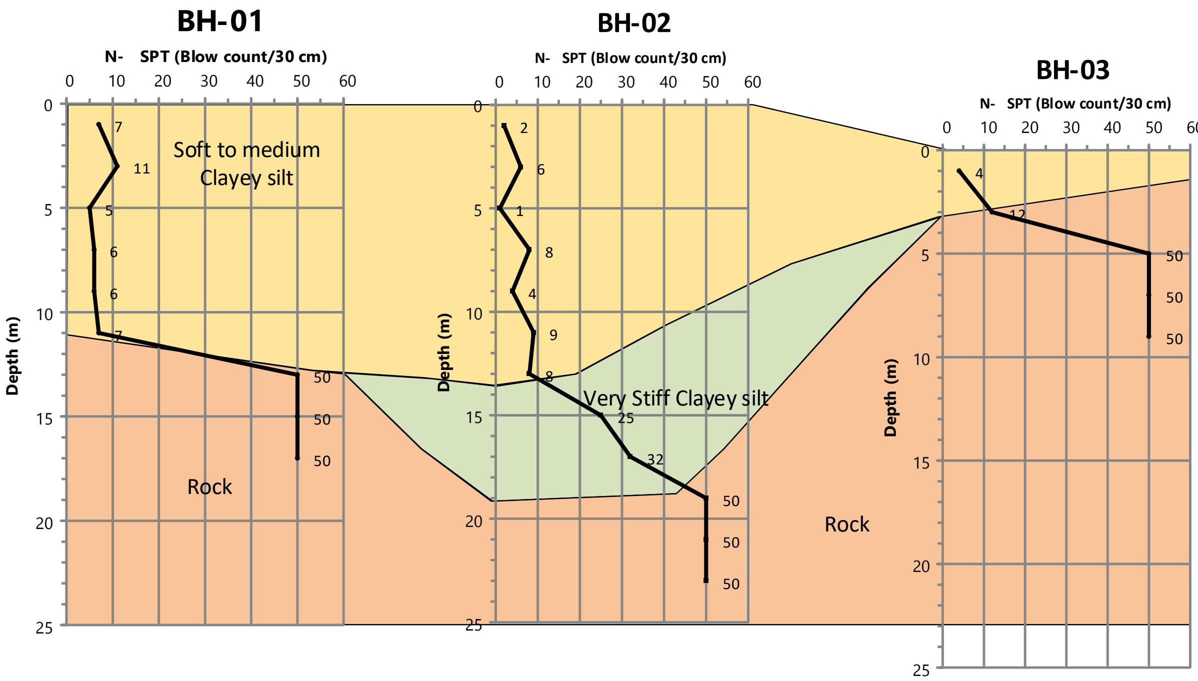

Figure 6. Soil layer according to borehole data.

Mapping of the slope contour after the landslide was conducted by using an unmanned aerial vehicle (UAV) or drone, as shown in Figure 7. The post-landslide slope contour through the photogrammetry method is shown in Figure 7. Figure 8 also shows the position of the first landslide, second landslide, and third landslide. The post-landslide slope contour could then be compared with the original slope contour in order to study the landslide-triggering mechanism. Based on the site investigations and the contours, the geometry of the slopes and soil stratifications are shown in Figure 9. Rainfall infiltration was modelled by using the flux boundary while overtopping was modelled by applying pressure head equal to 0 at the location where the overtopping was located, as shown in Figure 9a. Figure 9b shows the hydraulic boundary when there was no overtopping where only the flux boundary was applied. Figure 9c shows the post-failure slope geometry. The post-failure slope geometry is shown in Figure 9a,b to indicate the location of the sliding plane.

Table 3. Adopted Parameters for Simulation.

Soil Type	MaterialMmodel	k	Unit Weight (kN/m^3)	S_u (kPa)	c' (kPa)	ϕ' (°)	ϕ^b (°)
Volcanic Soil	Mohr–Coulomb	1×10^{-6}	18.8	-	10	26	13
Stiff Clay	Undrained (phi = 0)	1×10^{-8}	19	170	-	-	-
Bedrock	Bedrock (Impermeable)	1×10^{-9}	-	-	-	-	-

(**a**) (**b**)

Figure 7. Drone overview. ((**a**) drone; (**b**) orbit plan or flight pattern on grid).

Figure 8. Post-landslide slope contour.

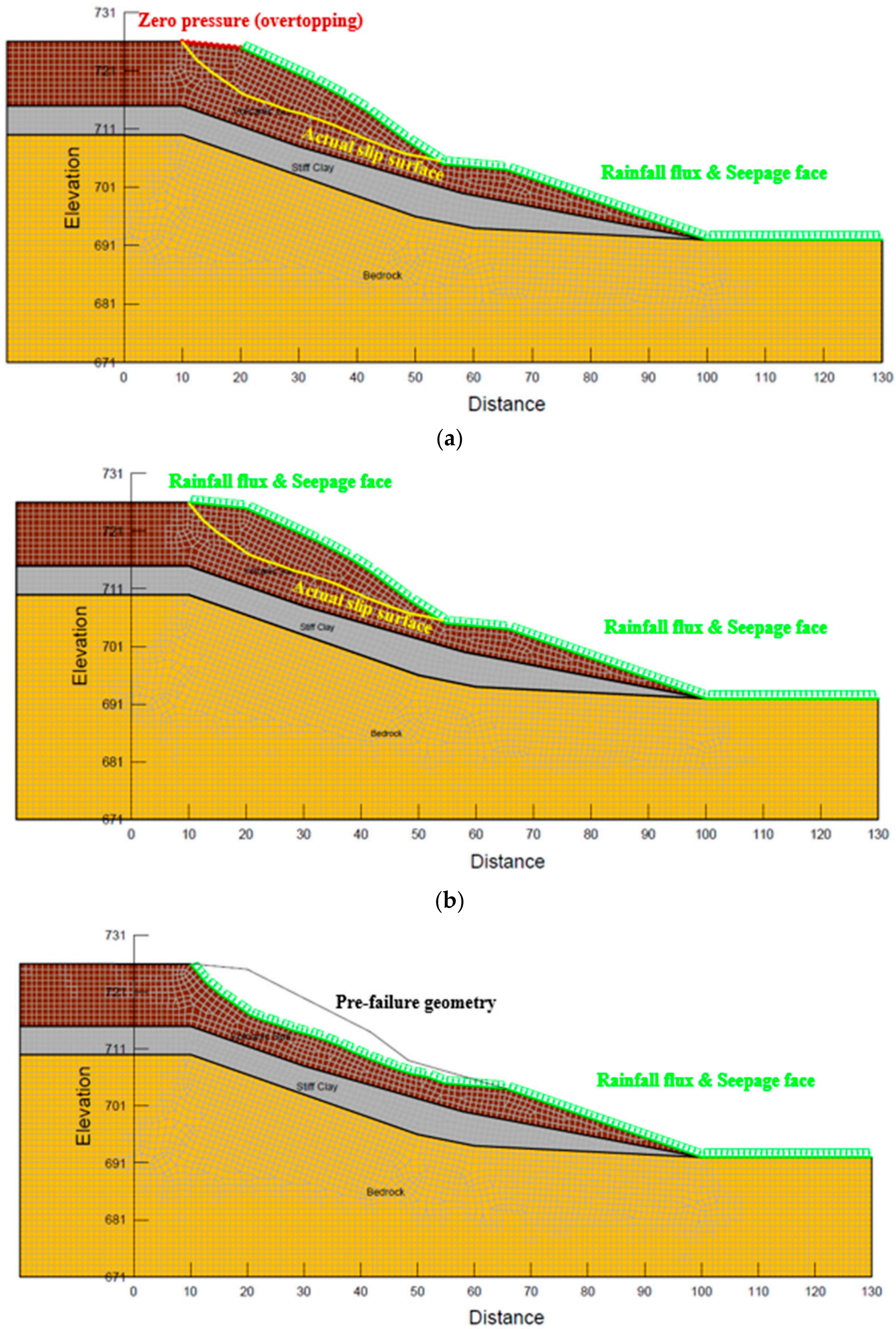

Figure 9. Slope geometry and soil stratifications. (**a**) With overtopping. (**b**) Without overtopping. (**c**) Post-failure geometry.

In order to assess the effect of rainfall infiltration in the unsaturated zone, it is important to determine the soil–water characteristic curve (SWCC), especially for the upper layer where the landslide occurred and which is sensitive to climate change. Aubertin, Mbonimpa [25] employed the pedotransfer function to estimate the SWCC of the upper layer based on basic soil properties which were obtained from laboratory tests which are shown in Table 2. For the second and third layers, typical SWCCs from the sample function available in Geostudio were adopted. Figure 10 shows the adopted SWCCs for the simulation.

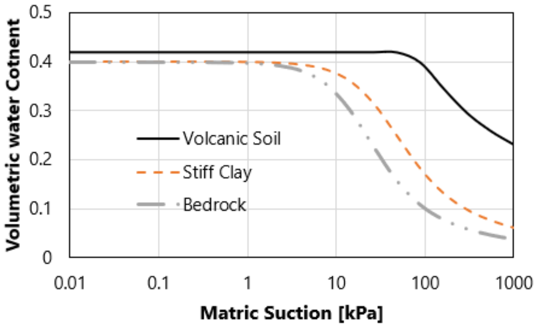

Figure 10. Estimated SWCC-θ.

The saturated coefficient permeability of soil was estimated from the saturated permeability database for volcanic soil collected by Wesley [36]. The saturated coefficient of permeability was then taken as 10^{-6} m/s for the upper layer, 10^{-8} m/s for the second layer, and 10^{-9} m/s for the third layer. Unsaturated permeability function was then determined from the SWCC and k_s by using the statistical method [31] and are shown in Figure 11. Grid and radius method in slope/W was adopted to determine the safety factor of the slope by assuming a circular slip surface.

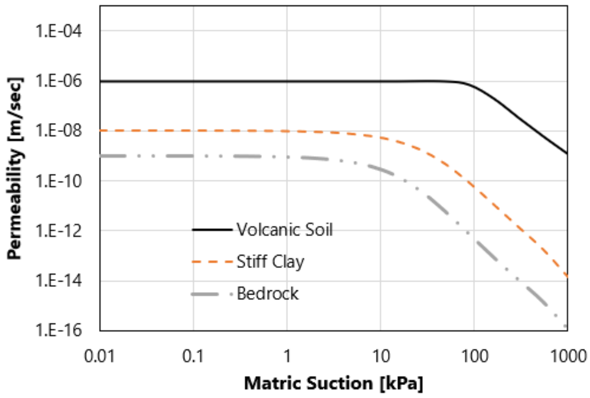

Figure 11. Permeability function based on Fredlund, Xing [31].

Inclinometers were installed at three locations as an early warning of potential hazards for public safety and provide an overview of the depth of the moving soil mass. The location of the inclinometer and illustration of the reading directions are shown in Figure 12. Only the inclinometer reading towards the slope direction A0 is shown.

The results of the three inclinometer readings are shown in Figures 13–15. The three inclinometer readings (IN-01, IN-02, and IN-03) show that there was no significant movement in the investigated site up to the present day. However, it is worth evaluating whether the slope remains stable under various rainfall infiltration rates and durations.

Parametric studies on the infiltration rates to the safety factor (SF) of the slope were conducted by applying a flux of 144 mm/day, 100 mm/day, 50 mm/day, and 30 mm/day. The rainfall was applied along the surface of the slope for a 1-day duration in order to determine critical rainfall duration under different flux.

Figure 12. Location of the inclinometer in Cimanggung slope failure.

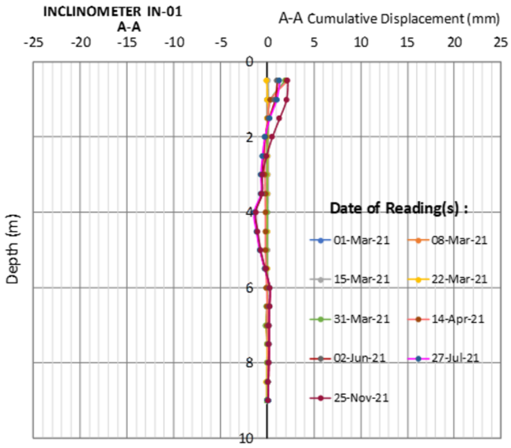

Figure 13. Inclinometer reading IN-01.

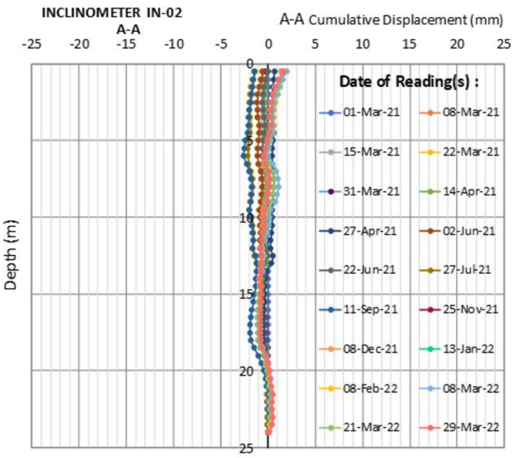

Figure 14. Inclinometer reading IN-02.

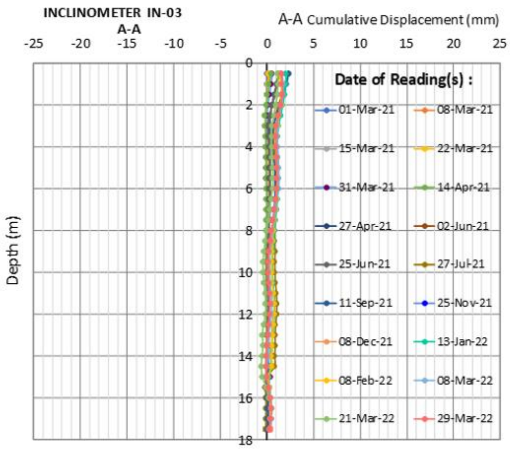

Figure 15. Inclinometer reading IN-03.

4. Results and Discussion

Figure 16 shows the slope failure contour after 4.5 h of rainfall with a flux of 144 mm/day with overtopping while Figure 17 shows the change in safety factor with time under different flux. The analysis shows that rainfall with flux of 144 mm/day will cause the slope to be under critical condition when the duration is approximately 4 h to 5 h. When the flux is 100 mm/day, 50 mm/day, and 30 mm/day, the duration required to reach SF equal to one will be longer. The slope contour matched with the post-failure contour. The triggering mechanism is indicated to be due to the decrease in soil suction and also due to an increase in the ground-water table. It is interesting to note that the phreatic line indicated by the blue dashed line raised up to the top of the slope. This phenomenon is not according to the site condition where the first crown was located somewhere below the drainage pipe.

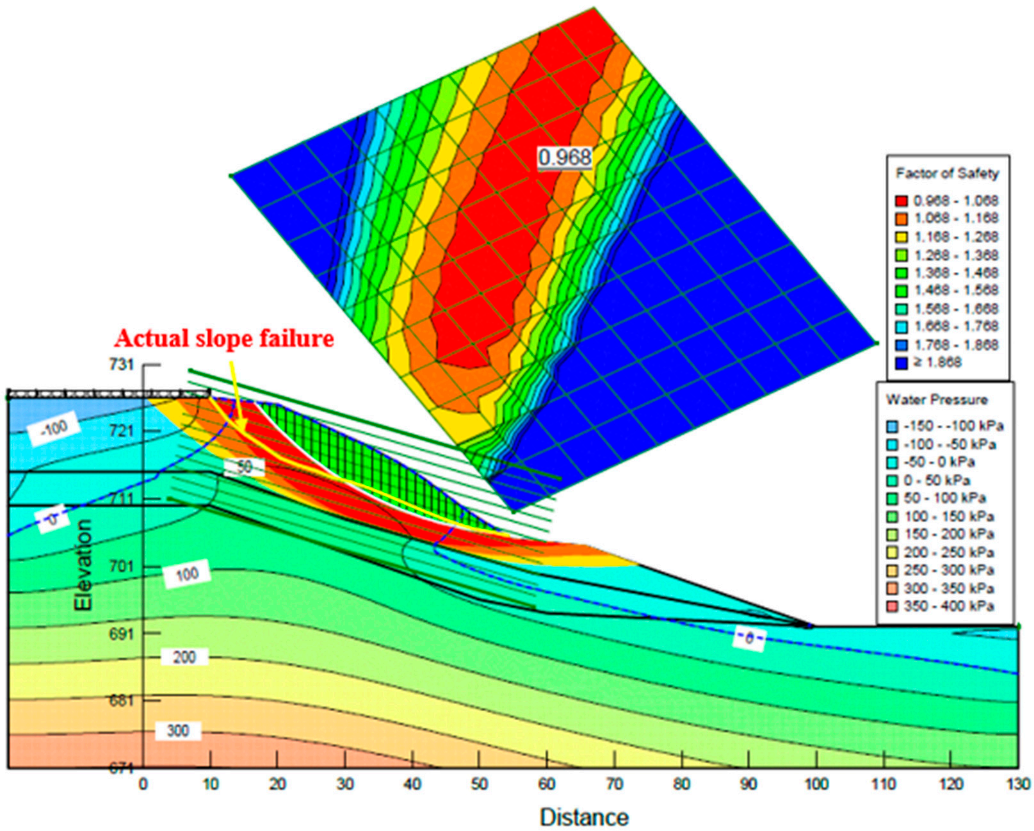

Figure 16. Slope failure after 4.5 h with a flux of 144 mm/day with overtopping.

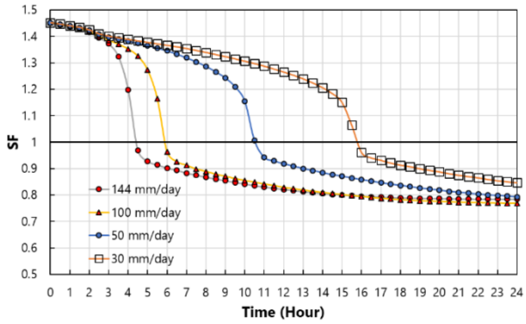

Figure 17. Change in safety factor with time under different flux.

Figure 18 shows the slip surface contour when the flux is 144 mm/day without considering broken drainage. It is shown that, without broken drainage, the phreatic line does not reach the top of the slope but reaches below the drainage pipe. The most critical slip surface appears to be more consistent with site observation where the first landslide occurs below the drainage pipe. Based on this analysis, the triggering mechanism for the first landslide is only the heavy rainfall and not the overtopping. The first landslide, induces progressive failure (second landslide) and damage to the drainage pipe which then causes overtopping. The red zone (zone with safety factor range from 0.981 to 1.081) appears to be quite consistent with the actual slip surface from the observation and hence indicates that progressive failure occurs as the second landslide is located inside the red zone.

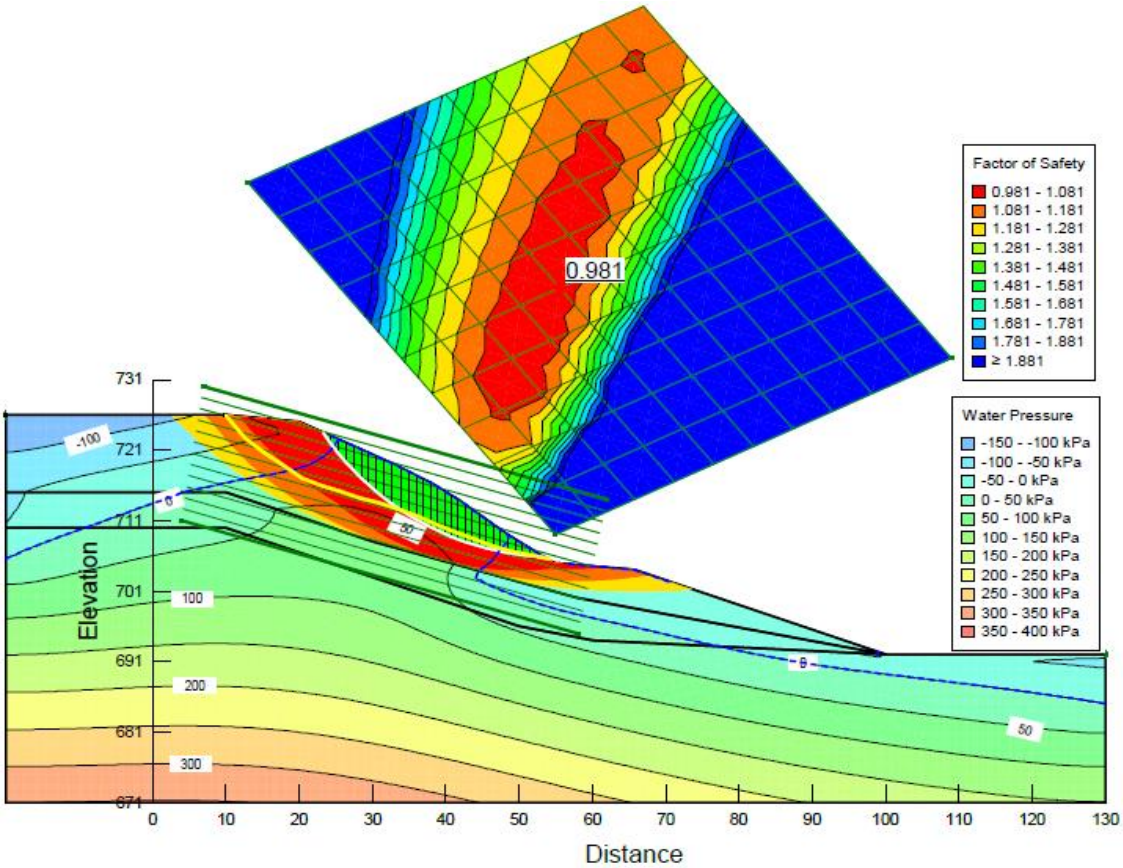

Figure 18. Slope failure after 5.5 h with a flux of 144 mm/day without overtopping.

Figure 19 shows the change in safety factor due to the infiltration without overtopping with time. It is shown that the change in safety factor with time does not differ much whether there is overtopping or not when the flux is high. However, as the flux, due to rainfall, decreases, the effect of infiltration due to overtopping becomes more prominent. This phenomenon is due to the infiltration rate, due to overtopping, being limited by the saturated permeability of the soil. For a better presentation, Figure 20 shows the critical duration (duration required to reach safety factor equals to one) and rainfall flux with and without overtopping. It is shown that with overtopping, the critical duration required under the same rainfall flux will be shorter, especially when the rainfall flux is lower.

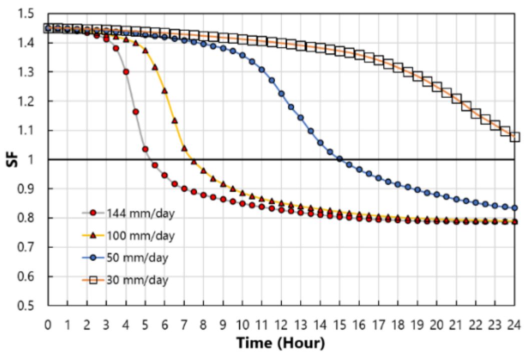

Figure 19. Change in safety factor with time under different flux without overtopping.

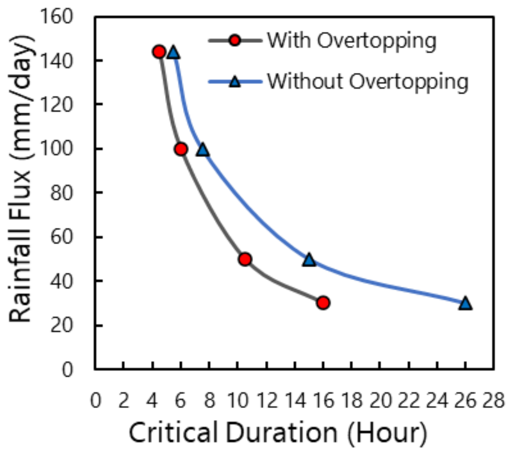

Figure 20. Critical duration under different rainfall infiltration.

Post-failure slope stability is also investigated in this paper. Figure 21 shows the stability of the slope when subjected to rainfall with a flux of 144 mm/day. Change in safety factor with time under different flux is shown in Figure 22. It can be seen that the slope remains stable even with 24 h of rainfall with a flux of 144 mm/day. While the soil properties remain the same, the slope has become much steeper and, hence, ground-water level does not raise significantly. Hence, post-failure slope geometry has a sufficient safety factor. This observation is consistent with the inclinometer reading where the movement of the slope is very small.

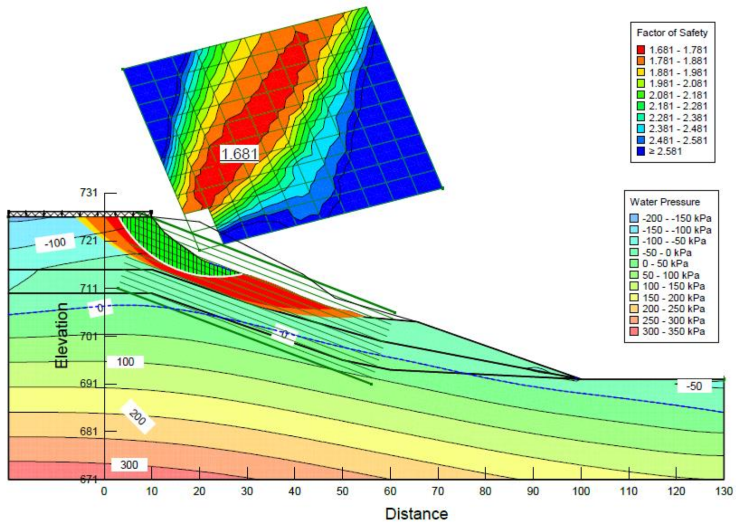

Figure 21. Post-failure stability after 4.5 h with a flux of 144 mm/day.

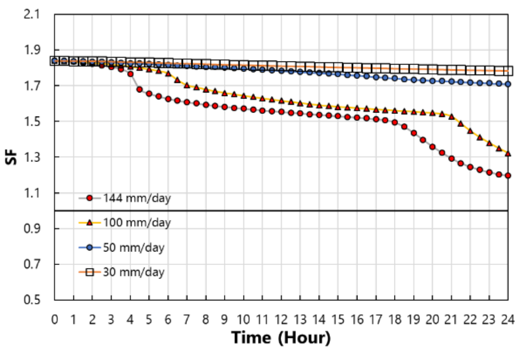

Figure 22. Change in safety factor with time under different flux for post-failure slope.

5. Conclusions

In this paper, the phenomenon which triggers slope failure at Cimanggung was investigated, and it is shown that a rational assessment can be made by estimating the unsaturated soil properties with limited soil data. It is shown that, when there is no overtopping, the slip surface appears to be more consistent with the site observation. Hence, according to the analysis which has been carried out, the triggering mechanism of the first landslide is heavy rainfall, with a rainfall flux of 144 mm/day, triggering the first landslide. Progressive failure then triggers the second landslide and, hence, damages the drainage pipe. While the unsaturated soil parameters were deduced based on some well-known correlation and databases, it can be seen that the triggering mechanism can be rationally estimated. Zones with a low safety factor from the analysis match very well with the actual slip surface that was observed at the site. The critical duration of slope failure can be reasonably estimated based on the parameters determined by using an empirical approach as the simulation shows that the safety factor of the slope with a flux of 144 mm/day will cause the slope to be under critical condition when the rainfall duration is approximately 4 h to 5 h, which matches with the testimony from the witnesses where slope failure occurs after 4 h of heavy rainfall. Slope stability of the post-failure geometry was also investigated. It is shown that the post-failure slope geometry has a higher safety factor when subjected to rainfall and is, hence, consistent with the instrumentation result.

Author Contributions: Conceptualization, M.W. and A.S (Alfrendo Satyanaga).; methodology, G.A.A. and A.S. (Andy Sugianto); software, G.A.A.; validation, A.H.H.; formal analysis, G.A.A.; investigation, A.S. (Alfrendo Satyanaga) and A.H.H.; resources, A.S. (Andy Sugianto); data curation, A.S. (Andy Sugianto); writing—original draft, G.A.A. and M.W.; writing—review and editing, P.P.R. and A.S.

(Alfrendo Satyanaga); visualization, A.H.H.; supervision, M.W. and P.P.R.; project administration, A.S. (Alfrendo Satyanaga) and A.H.H.; funding acquisition, A.S. (Alfrendo Satyanaga). All authors have read and agreed to the published version of the manuscript.

Funding: This research was funded by Nazarbayev University, 11022021CRP1512 and 20122022FD4133.

Institutional Review Board Statement: Not applicable.

Informed Consent Statement: Not applicable.

Data Availability Statement: Not applicable.

Acknowledgments: The authors would like to thank Parahyangan Catholic University for the support which was provided, and P.T. Geotechnical Engineering Consultant for providing the data, documentation, and visual inspection at the site.

Conflicts of Interest: The authors declare no conflict of interest.

References

1. Fredlund, D.G.; Rahardjo, H.; Fredlund, M.D. *Unsaturated Soil Mechanics in Engineering Practice*; John Wiley & Sons, Inc.: Hoboken, NJ, USA, 2012.
2. Fredlund, D.G.; Morgenstern, N.R.; Widger, R.A. The shear strength of unsaturated soils. *Can. Geotech. J.* **1978**, *15*, 313–321. [CrossRef]
3. Sun, D.-M.; Li, X.-M.; Feng, P.; Zang, Y.-G. Stability analysis of unsaturated soil slope during rainfall infiltration using coupled liquid-gas-solid three-phase model. *Water Sci. Eng.* **2016**, *9*, 183–194. [CrossRef]
4. Satyanaga, A.; Kim, Y.; Hamdany, A.H.; Nistor, M.-M.; Sham, A.W.L.; Rahardjo, H. Chapter 12—Preventive measures for rainfall-induced slope failures in Singapore. In *Climate and Land Use Impacts on Natural and Artificial Systems*; Nistor, M.-M., Ed.; Elsevier: Amsterdam, The Netherlands, 2021; pp. 205–223.
5. Rahardjo, H.; Ong, T.H.; Rezaur, R.B.; Leong, E.C. Factors Controlling Instability of Homogeneous Soil Slopes under Rainfall. *J. Geotech. Geoenviron. Eng.* **2007**, *133*, 1532–1543. [CrossRef]
6. Zhenlei, W.; Shang, Y.-Q.; Sun, H.-Y.; Xu, H.-D.; Wang, D.-F. The effectiveness of a drainage tunnel in increasing the rainfall threshold of a deep-seated landslide. *Landslides* **2019**, *16*, 1731–1744. [CrossRef]
7. Zhang, L.L.; Fredlund, M.D.; Fredlund, D.G.; Lu, H.; Wilson, G.W. The influence of the unsaturated soil zone on 2-D and 3-D slope stability analyses. *Eng. Geol.* **2015**, *193*, 374–383. [CrossRef]
8. Rahardjo, H.; Satyanaga, A.; Leong, E.; Din, F.; Song, N.; Looi, W. *Slope Failures in Singapore Due to Rainfall*; Nanyang Technological University: Singapore, 2007.
9. Sengani, F.; Mulenga, F. Influence of Rainfall Intensity on the Stability of Unsaturated Soil Slope: Case Study of R523 Road in Thulamela Municipality, Limpopo Province, South Africa. *Appl. Sci.* **2020**, *10*, 8824. [CrossRef]
10. Ijaz, N.; Ye, W.; Rehman, Z.u.; Dai, F.; Ijaz, Z. Numerical study on stability of lignosulphonate-based stabilized surficial layer of unsaturated expansive soil slope considering hydro-mechanical effect. *Transp. Geotech.* **2022**, *32*, 100697. [CrossRef]
11. Sun, H.-Y.; Wu, X.; Wang, D.-F.; Xu, H.-D.; Liang, X.; Shang, Y.-Q. Analysis of deformation mechanism of landslide in complex geological conditions. *Bull. Eng. Geol. Environ.* **2019**, *78*, 4311–4323. [CrossRef]
12. Ip, S.C.Y.; Rahardjo, H.; Satyanaga, A. Three-dimensional slope stability analysis incorporating unsaturated soil properties in Singapore. *Georisk Assess. Manag. Risk Eng. Syst. Geohazards* **2021**, *15*, 98–112. [CrossRef]
13. Das, P.; Bharat, T.V. Reconstruction of a wetting-induced shallow landslide in Shiillong, India. *Proc. Inst. Civ. Eng.* **2020**, *173*, 48–53.
14. Wijaya, M.; Leong, E.C. Discussion of "Permeability function for oil sands tailings undergoing volume change during drying". *Can. Geotech. J.* **2018**, *56*, 1–3. [CrossRef]
15. Zhang, F.; Wilson, G.W.; Fredlund, D.G. Permeability function for oil sands tailings undergoing volume change during drying. *Can. Geotech. J.* **2017**, *55*, 191–207. [CrossRef]
16. Mahmood, K.; Kim, J.M.; Ashraf, M.; Ziaurrehman. The effect of soil type on matric suction and stability of unsaturated slope under uniform rainfall. *KSCE J. Civ. Eng.* **2016**, *20*, 1294–1299. [CrossRef]
17. Brand, E.W. Slope instability in Tropical Areas. In Proceedings of the 6th International Symposium on Landslides, Christchurch, New Zealand, 10 February 1992; pp. 20131–22051.
18. Rahardjo, H.; Nio, A.S.; Eng Choon, L.; Ng Yew, S. Effects of Groundwater Table Position and Soil Properties on Stability of Slope during Rainfall. *J. Geotech. Geoenviron. Eng.* **2010**, *136*, 1555–1564. [CrossRef]
19. Yao, Y.; Li, J.; Xiao, Z.; Xiao, H. Soil-Water Characteristics and Creep Deformation of Unsaturated Expansive Subgrade Soil: Experimental Test and Simulation. *Front. Earth Sci.* **2021**, *9*, 1141. [CrossRef]
20. Wijaya, M.; Leong, E.C.; Rahardjo, H. Effect of shrinkage on air-entry value of soils. *Soils Found.* **2015**, *55*, 166–180. [CrossRef]
21. Wijaya, M.; Leong, E.C. Equation for unimodal and bimodal soil–water characteristic curves. *Soils Found.* **2016**, *56*, 291–300. [CrossRef]

22. Hamdany, A.H.; Shen, Y.; Satyanaga, A.; Rahardjo, H.; Lee, T.-T.D.; Nong, X. Field instrumentation for real-time measurement of soil-water characteristic curve. *Int. Soil Water Conserv. Res.* **2022**, *10*, 586–596. [CrossRef]
23. Ijaz, N.; Rehman, Z.u.; Ijaz, Z. Recycling of paper/wood industry waste for hydromechanical stability of expansive soils: A novel approach. *J. Clean. Prod.* **2022**, *348*, 131345. [CrossRef]
24. Kovacs, G. *Seepage Hydraulics*, 1st ed.; Elsevier: Amsterdam, The Netherlands, 1981.
25. Aubertin, M.; Mbonimpa, M.; Bussière, B.; Chapuis, R.P. A model to predict the water retention curve from basic geotechnical properties. *Can. Geotech. J.* **2003**, *40*, 1104–1122. [CrossRef]
26. Chin, K.B.; Leong, E.C.; Rahardjo, H. A simplified method to estimate the soil-water characteristic curve. *Can. Geotech. J.* **2010**, *47*, 1382–1400. [CrossRef]
27. *SoilVision*; SoilVision System Ltd.: Saskatoon, SK, Canada, 2003.
28. Nemes, A.; Schaap, M.; Leij, F.; Wösten, J. *UNSODA 2.0: Unsaturated Soil Hydraulic Database. Database and Program for Indirect Methods of Estimating Unsaturated Hydraulic Properties*, 2nd ed.; US Salinity Laboratory, ARS, USDA: Washington, DC, USA, 2018.
29. Nemes, A.; Schaap, M.G.; Leij, F.J.; Wösten, J.H.M. Description of the unsaturated soil hydraulic database UNSODA version 2.0. *J. Hydrol.* **2001**, *251*, 151–162. [CrossRef]
30. Fredlund, D.G.; Xing, A. Equations for the soil-water characteristic curve. *Can. Geotech. J.* **1994**, *31*, 521–532. [CrossRef]
31. Fredlund, D.G.; Xing, A.; Huang, S. Predicting the permeability function for unsaturated soils using the soil-water characteristic curve. *Can. Geotech. J.* **1994**, *31*, 533–546. [CrossRef]
32. UInspire. *Situation Report #8 Rrespon Bencana Longsor Kampung Daud/Bojong Kondang, Desa Cihanjuang, Kec. Cimanggung, Kab. Sumedang, Prov. Jawa Barat*; UInspire: Sumedang, Indonesia, 2020.
33. Bar, N.; Kostadinovski, M.; Tucker, M.; Byng, G.; Rachmatullah, R.; Maldonado, A.; Pötsch, M.; Gaich, A.; McQuillan, A.; Yacoub, T. Rapid and robust slope failure appraisal using aerial photogrammetry and 3D slope stability models. *Int. J. Min. Sci. Technol.* **2020**, *30*, 651–658. [CrossRef]
34. Gonizzi Barsanti, S.; Remondino, F.; Visintini, D. 3D Surveying and Modeling of Archaeological Sites—Some Critical Issues. *ISPRS Ann. Photogramm. Remote Sens. Spat. Inf. Sci.* **2013**, *II-5/W1*, 145–150. [CrossRef]
35. Manousakis, J.; Zekkos, D.; Saroglou, H.; Kallimogiannis, V.; Bar, N. Analysis of slope instabilities in the Corinth Canal using UAV-enabled mapping. In Proceedings of the ICONHIC 2nd International Conference on Natural Hazards & Infrastructure, Chania, Greece, 23–26 June 2019.
36. Wesley, L.D. *Geotechnical Engineering in Residual Soils*; John Wiley & Sons: Hoboken, NJ, USA, 2010.